physica status solidi

pss

www.pss-journals.com

reprint

WILEY-VCH

Phys. Status Solidi B **253**, No. 2, 384–391 (2016) / **DOI** 10.1002/pssb.201552138

physica status solidi b
www.pss-b.com
basic solid state physics

Ferroelectricity in $(Pb_ySn_{1-y})_2P_2S_6$ mixed crystals and random field BEG model

K. Z. Rushchanskii[1], R. M. Bilanych[2], A. A. Molnar[2], R. M. Yevych[*,2], A. A. Kohutych[2], S. I. Perechinskii[2], V. Samulionis[3], J. Banys[3], and Y. M. Vysochanskii[2]

[1] Peter Grünberg Institut, Quanten-Theorie der Materialien, Forschungszentrum Jülich and JARA, D-52425 Jülich, Germany
[2] Institute for Physics and Chemistry of Solid State, Uzhgorod National University, 88000 Uzhgorod, Ukraine
[2] Faculty of Physics, Vilnius University, Sauletekio 9/3, LT-10222 Vilnius, Lithuania

Received 15 March 2015, revised 19 September 2015, accepted 22 September 2015
Published online 23 October 2015

Keywords Blume–Emery–Griffiths model, ferroelectrics, phase diagrams, tricritical point

[*] Corresponding author: e-mail ryevych@gmail.com, Phone/Fax: +380-31-2232339

In $Sn_2P_2S_6$ ferroelectric under compression, the second-order phase transition line is observed down to the tricritical point as the transition temperature decreases to 250 K. A tricriticality at a similar temperature is also revealed in the mixed crystals on S→Se substitution. For the mixed crystals with Sn→Pb substitution, ultrasound, hypersound, and low-frequency dielectric studies also show heterophase features appearing on decrease of the ferroelectric transition temperature below a so-called "waterline temperature" near 250 K. Such behavior agrees with the Blume–Emery–Griffiths (BEG) model appropriate for the ferroelectric system under investigation with a three-well local potential for the order parameter fluctuations. The BEG model modified by the random-field phase diagram in the vicinity of the tricritical point qualitatively explains the influence of the cationic substitution on the $(Pb_ySn_{1-y})_2P_2S_6$ ferroelectric properties.

1 Introduction $Sn_2P_2S_6$ crystal is a uniaxial ferroelectric with a three-well local potential for order-parameter fluctuations [1]. This potential can be related to Blume–Emery–Griffiths (BEG) model for analysis of systems with 0 and ±1 pseudospin [2–4]. Such a model predicts the possibility of a tricritical point (TCP) in state diagrams where a line of second-order phase transitions (PT) is transformed into a first-order transition line. This point can be observed as the transition temperature decreases due to pressure or by variation of chemical composition. In addition to the first-order transition line, at least metastable paraelectric and ferroelectric states are also predicted [3]. Moreover, the phase diagram could also be complicated, for example, by quadrupole-state occurrences [4].

In mixed crystals, random bond and random field defects can strongly affect the phase diagram that is predicted by the BEG model. The TCP coordinates can be shifted and a segment of the formerly known first-order transition line can be observed as continuous transitions [5]. In the vicinity of the TCP polarization, anisotropy decreases because of the free-energy surface flattening [6], which confirms the influence of disorder factors in mixed crystals. In addition, regions of dipole glass or ferroglass regions can appear in the phase diagram [7].

Under compression, the second-order ferroelectric transition in $Sn_2P_2S_6$ obviously changes its character to the first order at $p \approx 0.4$ GPa and $T \approx 250$ K, as follows from the analysis of the ultrasound-temperature anomalies [8]. Neutron diffraction data show [9] that under a pressure of 0.6 GPa, the tricritical point is reached in the temperature–pressure ferroelectric phase diagram. High-resolution X-ray diffraction temperature measurements at different pressures also clearly demonstrate the first-order character of the ferroelectric transition in $Sn_2P_2S_6$ crystals under a pressure of 1.2 GPa where the transition temperature decreases to 110 K [10].

On S→Se substitution in $Sn_2P_2(Se_xS_{1-x})_6$ mixed crystals, the TCP on the phase diagram is located at $x \approx 0.6$ and $T \approx 240$ K [11]. Here, the TCP is a virtual one because the incommensurate phase appears at $x \geq x_{LP} \approx 0.28$ (x_{LP} is the Lifshitz point coordinate) [12].

The three-well potential in $Sn_2P_2S_6$ crystals is related to the stereoactivity of Sn^{2+} cation $5s^2$ electron lone pairs [1]. With substitution of sulfur by selenium, the covalence of the chemical bonds increases and results in a weaker intercell

interaction at a basically similar form of the local three-well potential, the temperature of the ferroelectric transition being decreased. Under compression, the chemical-bond ionicity increases and the stereoactivity of Sn^{2+} cations weakens. This fact determines the strong transformation of the local three-well potential—the side wells become flatter, which naturally reduces the temperature of the ferroelectric transition and helps reduce the TCP to near 250 K.

It is interesting to elucidate the evolution of the ferroelectric transition with substitution of tin by lead in $(Pb_ySn_{1-y})_2P_2S_6$ mixed crystals. In the case of $PbTiO_3$ crystal, the stereoactivity of the Pb $6s^2$ electron lone pair together with the covalence of the Ti–O bonds determines the strongest ferroelectricity in the family of oxide perovskites. However, the energy distance between the Pb 6s orbitals and the S 3p orbitals in chalcogenide materials is larger in comparison with the distance to the energy levels of O 2p orbitals in $PbTiO_3$. Hence naturally, the stereoactivity of double-charged lead cations in chalcogenides is expected to be weaker than in the oxide case, and it can also be smaller compared to the tin cation stereoactivity. For $Pb_2P_2S_6$, the paraelectric state can be stable down to the lowest temperatures. In the first structural study [13], the $P2_1/c$ space group was reported for $Pb_2P_2S_6$ crystals, but later an acentric Pn structure at room temperature was proposed [14]. Experimental pyroelectric and piezoelectric studies support the former conclusion about the centrosymmetric structure of $Pb_2P_2S_6$ crystal at room temperature [15]. Also, Raman scattering spectroscopy shows an increase of the $Pb_2P_2S_6$ lattice anharmonicity with cooling: the frequency of the lowest-energy optical phonon slightly decreases on temperature decrease [15]. This finding can be interpreted as a possibility of a virtual or very-low-temperature ferroelectric phase transition in $Pb_2P_2S_6$ crystal. Consequently, Pb^{2+} cations obviously have some "residual" stereoactivity in the $Pb_2P_2S_6$ lattice.

In $(Pb_ySn_{1-y})_2P_2S_6$ mixed crystals, with increasing lead concentration the ferroelectric transition temperature goes down to 4.2 K at $y = 0.61$ [15]. Besides, low-temperature ferroelectric ordering or possibly dipole glass states were evidenced at $y > 0.61$ by dielectric studies [16]. As a whole, $(Pb_ySn_{1-y})_2P_2S_6$ mixed crystals present a good possibility for a dipole-ordering study in a system that can be described within the BEG model with random fields. In crystals of the $Sn_2P_2S_6$ family, metal cations are located in general positions, substitution of tin by lead breaks down the inversion symmetry of the unit cell and induces randomly distributed electric dipoles.

In the present paper, we present low-frequency dielectric, ultrasound, and hypersound Brillouin scattering studies of $(Pb_ySn_{1-y})_2P_2S_6$ mixed crystals that give evidence for the TCP being reached at $y > 0.2$ and coexistence of phases in the temperature–composition (T–y) phase diagram. The obtained experimental data are compared with the BEG model that predicts obligatory transformation of the second-order phase transitions into the first-order ones on the transition-temperature decrease and smearing of some segment of the first-order transition line under the random field influence [5].

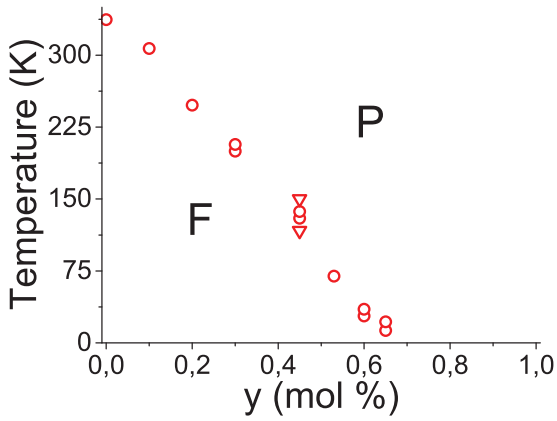

Figure 1 Phase-transition temperature vs. volume fraction of lead atoms in $(Pb_ySn_{1-y})_2P_2S_6$ mixed crystal (P: paraelectric phase, F: ferroelectric phase). The temperature positions of two dielectric and ultrasound anomalies are shown for the $y = 0.3$ and $y = 0.45$ compositions. For the $y = 0.45$ composition, the range of the temperature hysteresis and possible phase coexistence is shown by triangles. For the compositions with $y = 0.53$, 0.61, and 0.66, the positions of the dielectric anomalies are shown according to the data of Ref. [16].

2 Experimental Dielectric susceptibility was investigated by a Goodwill LCR-815 at a frequency of 10^4 Hz with a temperature variation rate of 0.1 K min^{-1}. The investigated samples were prepared as plates with $5 \times 5 \times 3$ mm^3 dimensions with silver paste electrodes on the largest (001) faces that were nearly normal to the spontaneous polarization direction.

The Brillouin scattering spectra were studied using a He–Ne laser and a pressure-scanned three-pass Fabry–Perot interferometer with the sharpness of 35 and the free spectral range of 2.51 cm^{-1}. The scattered light in the $Y(XX)\bar{Y}$ geometry was collected from the bulk of the investigated samples. The samples were placed in a UTREX cryostat, in which the temperature was stabilized with an accuracy of about 0.3 K [18].

The measurements of the longitudinal ultrasonic velocity and attenuation were performed using a computer-controlled pulse-echo equipment [19]. The precision of the relative velocity measurements was better than 10^{-4}. The temperature stabilization was better than 0.02 K. The sample was carefully polished to have precisely parallel faces normal to the Y-axis. Silicone oil was used as an acoustic bond for the longitudinal ultrasonic waves. The measurements were carried out at 10 MHz frequency using piezoelectric $LiNbO_3$ transducers. Vapor-transport technology was used for the growth of $(Pb_ySn_{1-y})_2P_2S_6$ single crystals. For the samples prepared, the Cartesian axes X and Y coincide with [100] and [010] crystallographic directions.

The dielectric susceptibility, ultrasound, and hypersound velocity temperature anomalies were used to determine the compositional dependence of the ferroelectric phase-transition temperature for $(Pb_ySn_{1-y})_2P_2S_6$ mixed crystals. These data together with previously obtained results are shown in Fig. 1. With increasing lead concentration to $y =$

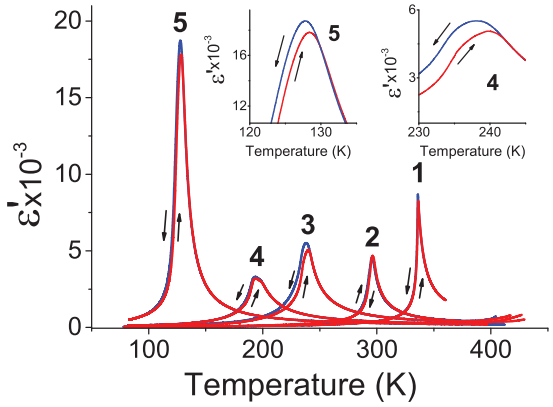

Figure 2 Temperature dependence of the real part of dielectric susceptibility at 10^4 Hz on cooling (blue lines) and heating (red lines) for $(Pb_ySn_{1-y})_2P_2S_6$ mixed crystals with $y = 0 - 1$; 0.1 – 2; 0.2 – 3; 0.3 – 4; 0.45 – 5. The temperature hysteresis for different y is shown in the insets.

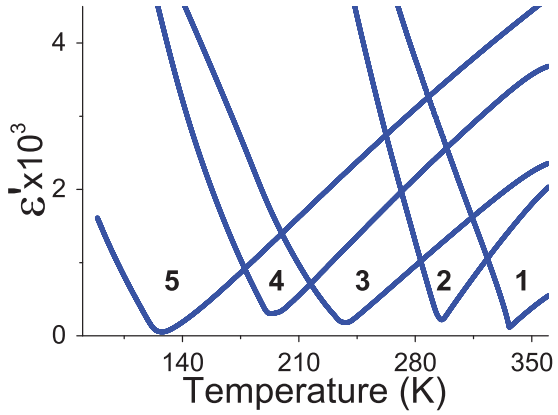

Figure 4 Temperature dependence of the reciprocal real part of dielectric susceptibility on cooling at 10^4 Hz for $(Pb_ySn_{1-y})_2P_2S_6$ mixed crystals with $y = 0 - 1$; 0.1 – 2; 0.2 – 3; 0.3 – 4; 0.45 – 5.

0.2, the temperature of the second-order phase transition T_0 decreases to about 248 K (Figs. 2 and 3). At $y \gtrsim 0.2$, the ferroelectric transition obviously changes its character to the first order, which can be seen from the transformation of the low-frequency dielectric susceptibility temperature anomalies (Fig. 2). For the sample with $y = 0.3$, the anomalies of the real and imaginary parts of dielectric susceptibility become broader and have a clear temperature hysteresis. For these compositions, the temperature dependence of dielectric losses is smeared into ferroelectric phase. For $y = 0.45$, the dielectric losses have the highest value near the first-order phase transition and their temperature dependence has a shape of an almost symmetric maximum (Fig. 3).

The temperature dependence of reciprocal dielectric susceptibility (Fig. 4) for pure $Sn_2P_2S_6$ compound demonstrates the ratio of slopes in the ferroelectric and paraelectric phases near 4, which shows proximity to the tricritical point. For the mixed crystals, the slopes are almost equal and cannot be described by a simple picture of a continuous phase transition.

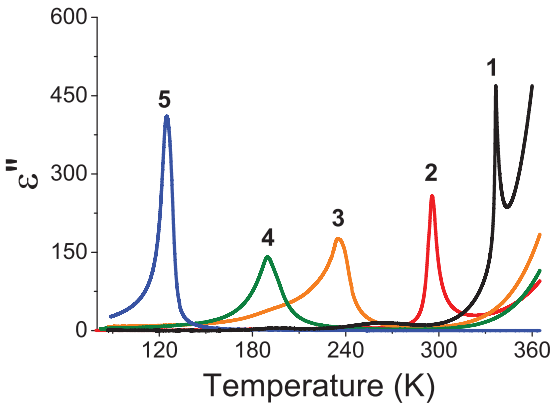

Figure 3 Temperature dependence of the imaginary part of dielectric susceptibility on cooling at 10^4 Hz for $(Pb_ySn_{1-y})_2P_2S_6$ mixed crystals with $y = 0 - 1$; 0.1 – 2; 0.2 – 3; 0.3 – 4; 0.45 – 5.

For the samples with $y = 0.1$ and 0.2, the temperature dependence of the ultrasound attenuation is similar to the one expected from the Landau-Khalatnikov model for second-order phase transitions—it is seen as an asymmetric peak with maximal values near 6 cm^{-1}, and with temperature widths (at 3 cm^{-1} level) near 2 and 4 K, respectively (Fig. 10). For the increased content of lead, in the mixed crystal with $y = 0.3$, the ultrasound anomalies are qualitatively changed—here an additional inflection appears at the step of the sound velocity (Fig. 5a) and the attenuation temperature

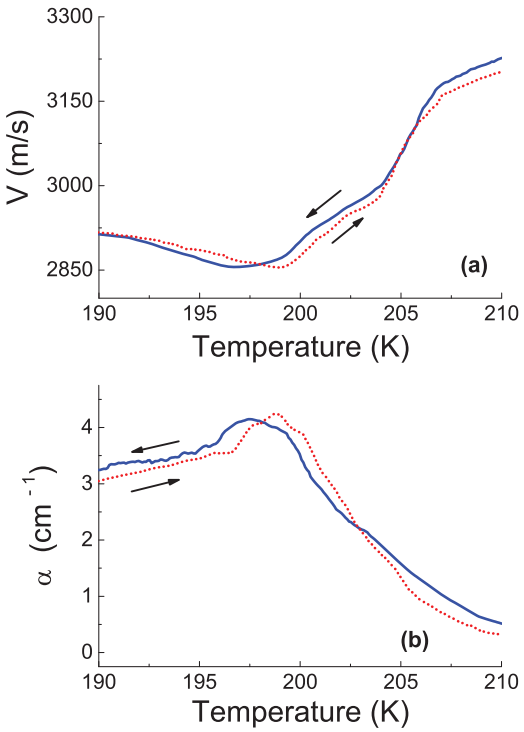

Figure 5 Temperature dependences of ultrasound velocity (a) and attenuation (b) on cooling (blue solid lines) and heating (red dotted lines) in the phase-transition region for a $(Pb_{0.3}Sn_{0.7})_2P_2S_6$ crystal.

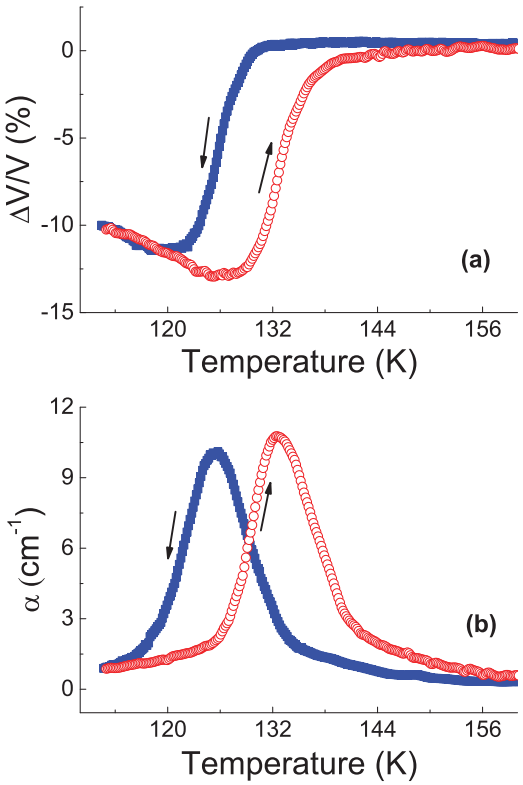

Figure 6 Temperature dependences of ultrasound velocity (a) and attenuation (b) at cooling (blue solid symbols) and heating (red open symbols) in the phase transition region for $(Pb_{0.45}Sn_{0.55})_2P_2S_6$ crystals.

maximum is smeared into both the paraelectric and ferroelectric phases (Fig. 5b). One can suppose that the first-order transition occurs already for the $y = 0.3$ composition and the phase coexistence leads to a complication of the sound-velocity anomaly and smearing of the attenuation maximum.

For the $y = 0.45$ mixed crystal, the temperature hysteresis of the dielectric susceptibility and the sound velocity is clearly observed (Fig. 2, Fig. 6) which is related to the first-order character of the ferroelectric phase transition near 132 K. For the ultrasound velocity and attenuation anomalies, the temperature hysteresis equals about 10 K. In the heating mode, the temperature dependences of the sound velocity and attenuation have anomalous smearing into the paraelectric phase within an interval of above 10 K. The temperature maximum of attenuation is 10 cm^{-1} on cooling and 11 cm^{-1} on heating. In both regimes, this maximum has the temperature width of about 30 K. A broader temperature hysteresis of the ultrasound anomalies at 10^7 Hz (Fig. 6) compared with the temperature hysteresis of the dielectric anomalies (10^4 Hz) (Fig. 2) can be related to the transformation of the distribution of relaxation times that is determined by spatial inhomogeneity of spontaneous polarization.

Using the Landau theory of second-order PT, one can describe the sound-velocity and attenuation anomalies. For the case of a one-component order parameter and its interaction with strain, the thermodynamical potential can be presented in the following form:

$$\Phi = \Phi_0 + \frac{1}{2}\alpha P^2 + \frac{1}{4}\beta P^4 + \frac{1}{6}\gamma P^6 + c_{ij}u_i u_j + q_{11i}u_i P^2 + r_{11ij}u_i u_j P^2 + \cdots \quad (1)$$

Here, $\alpha = \alpha_T(T - T_0)$, β, and γ are independent of temperature, c_{ij} are elastic moduli, q_{ijk} are electrostriction coefficients, r_{ijkl} are biquadratic electrostriction coefficients. In the approximation of one relaxation time $\tau = \tau_0/(T - T_0)$ for the order parameter dynamics, as supposed in the Landau–Khalatnikov model [20], the following expressions for the temperature dependence of the sound velocity and attenuation can be obtained:

$$V_{ij}^2 = V_{ij\infty}^2 - \frac{1}{1+\omega^2\tau^2}\left[\frac{2q_{11i}q_{11j}}{\rho\beta\sqrt{1-\frac{4\alpha\gamma}{\beta^2}}} + \frac{r_{11ij}\beta}{2\gamma\rho}\left(\sqrt{1-\frac{4\alpha\gamma}{\beta^2}}-1\right)\right], \quad (2)$$

$$\alpha = \frac{V_\infty^2 - V^2}{2V^3}\omega^2\tau\,. \quad (3)$$

Analysis of the temperature dependence of the longitudinal sound velocity propagating along the [010] direction in $(Pb_ySn_{1-y})_2P_2S_6$ crystals (Figs. 7 and 9) was performed using Eq. (2) with the values of the coefficients β and γ for the thermodynamic potential of Eq. (1) shown in Fig. 11. It should be noted that the α_T coefficient is almost independent of concentration and its value is about 1×10^6 J m C^{-2} K^{-1} and 1.25×10^6 J m C^{-2} K^{-1} from hypersound and ultrasound experiments, respectively. It was found that for all compositions at the description of the hypersound velocity anomalies, the electrostriction characteristics $q_{112} = 3.4 \times 10^9$ J m C^{-2} and $r_{1122} = 0.1 \times 10^{10}$ N m^2 C^{-2} can be used. For fitting of the ultrasound velocity anomalies, the values $q_{112} = 3.2 \times 10^9$ J m C^{-2} and $r_{1122} = 6.6 \times 10^{10}$ N m^2 C^{-2} were used. The temperature dependence of the relaxation time is characterized by the values of the τ_0 coefficient that are also shown in Fig. 11.

The ultrasound and hypersound attenuation calculated by Eq. (3) for the ferroelectric phase (Figs. 8 and 10) for all compositions of mixed crystals are higher than the experimentally observed attenuation data. This overestimation can be corrected by taking account of several relaxation times and mode Gruneisen coefficients. These coefficients are more appropriate as the interaction parameters than the electrostrictive coefficients, as was earlier discussed in details for pure $Sn_2P_2S_6$ crystals [21]. On cooling in ferroelectric phase, additional sound attenuation by domain walls can be observed as well [21].

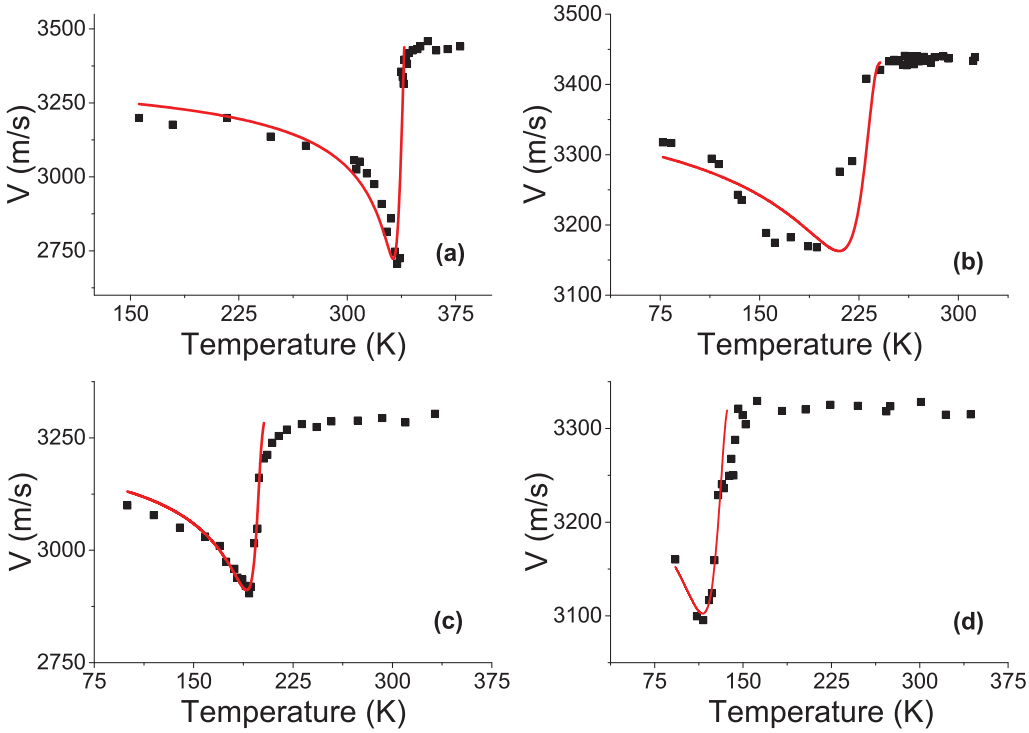

Figure 7 Temperature dependences of hypersound velocity for $(Pb_ySn_{1-y})_2P_2S_6$ crystals (symbols) and fitting of their anomalies (lines) by the Landau–Khalatnikov model (Eq. (2)): (a) $y = 0$; (b) $y = 0.2$; (c) $y = 0.3$; (d) $y = 0.45$.

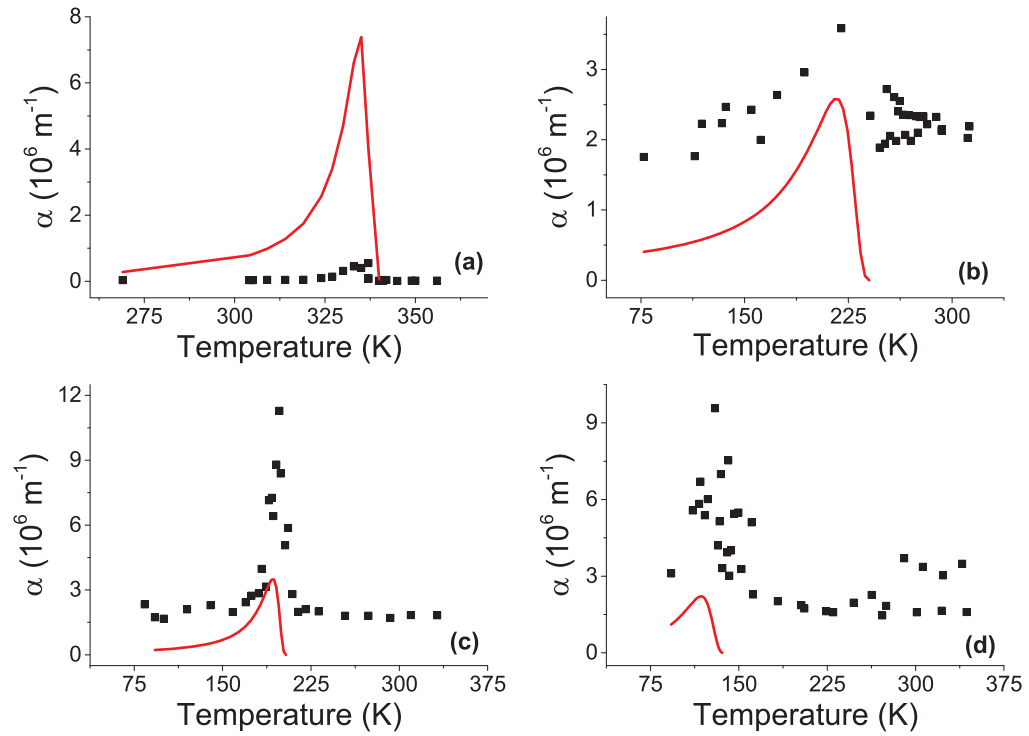

Figure 8 Temperature dependences of hypersound attenuation for $(Pb_ySn_{1-y})_2P_2S_6$ crystals (symbols) and their fitting of anomalies (lines) by the Landau–Khalatnikov model (Eq. (3)): (a) $y = 0$; (b) $y = 0.2$; (c) $y = 0.3$; (d) $y = 0.45$.

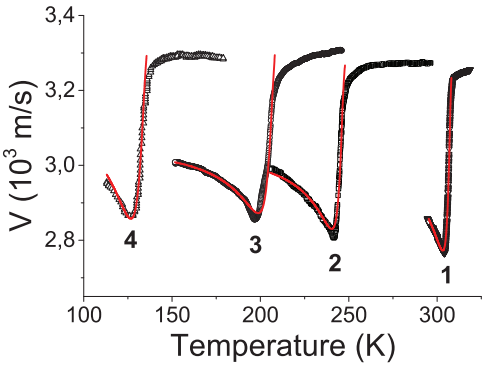

Figure 9 Temperature dependences of ultrasound velocity for $(Pb_ySn_{1-y})_2P_2S_6$ crystals (black symbols) and fitting of their anomalies (red lines) by the Landau–Khalatnikov model (Eq. (2)): 1 – $y = 0.1$; 2 – $y = 0.2$; 3 – $y = 0.3$; 4 – $y = 0.45$.

3 Discussion The anomalous growth of the hypersound attenuation at 10^9 Hz for the $y = 0.3$ composition (Fig. 8) can be related to sufficiently small and fast heterophase fluctuations in the vicinity of the first-order ferroelectric phase transition. For the $y = 0.45$ sample, the heterophase fluctuations become more extended and slower and are involved in the relaxation processes at lower frequencies which is demonstrated by the strong growth of the dielectric losses at 10^4 Hz (Fig. 3) and the ultrasound attenuation at 10^7 Hz (Fig. 10).

In addition, the relaxation time increase with substitution of tin by lead substitution (Fig. 11) is obviously related to strongly anharmonic order parameter dynamics in the local three-well potential for phase transitions near the TCP, which is achieved between $y = 0.2$ and 0.3 at the temperature of about 240 K.

The TCP location in the T–P diagram for $Sn_2P_2S_6$, in the T–x diagram for $Sn_2P_2(Se_xS_{1-x})_6$, and in the T–y diagram for $(Pb_ySn_{1-y})_2P_2S_6$ mixed crystals are compared in Fig. 13. For $Sn_2P_2S_6$ crystal, the TCP is obviously located at $P \gtrsim 0.4$ GPa and $T \lesssim 250$ K [8], for $Sn_2P_2(Se_xS_{1-x})_6$ solid solutions the virtual TCP (inside the incommensurate phase)

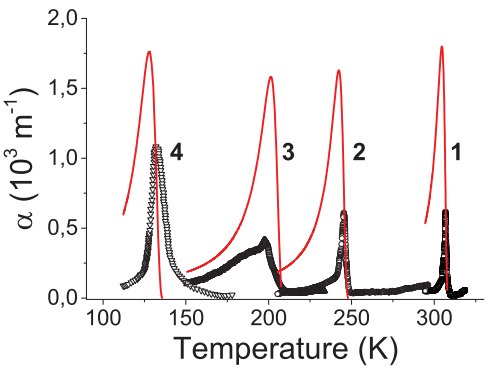

Figure 10 Temperature dependences of ultrasound attenuation for $(Pb_ySn_{1-y})_2P_2S_6$ crystals (black symbols) and fitting of their anomalies (red lines) by the Landau–Khalatnikov model (Eq. (3)): 1 – $y = 0.1$; 2 – $y = 0.2$; 3 – $y = 0.3$; 4 – $y = 0.45$.

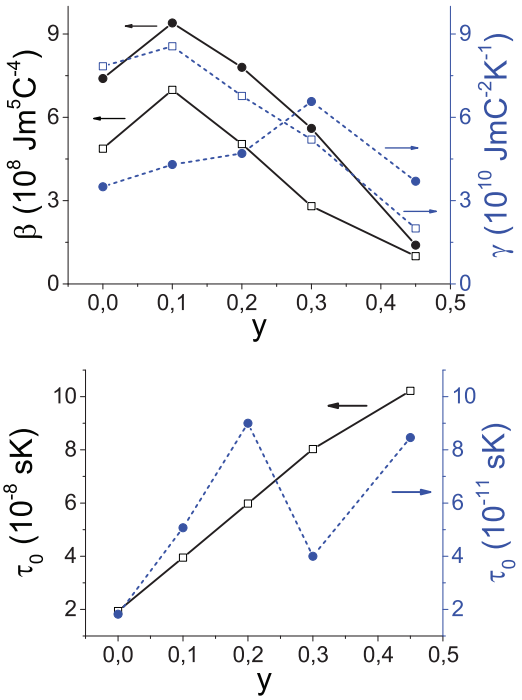

Figure 11 Compositional dependences of β and γ coefficients (the top panel) of the thermodynamic potential (Eq. (1)) and prefactor τ_0 (the bottom panel) from the temperature dependence of the relaxation time obtained from the analysis of the temperature anomalies of the ultrasound (open symbols) and hypersound (solid symbols) velocities and attenuation in the Landau–Khalatnikov model (Eqs. (2) and (3)).

was predicted to be placed at $x \approx 0.6$ and $T \approx 240$ K [11, 12]. It is intriguing that for $(Pb_ySn_{1-y})_2P_2S_6$ mixed crystals, the TCP can also be placed at a similar temperature—near 240 K at $y > 0.2$.

For the diluted BEG model, a segment of the former firs-order transition line (just below the TCP in the ideal system) becomes a disorder-induced continuous transition line (Fig. 12) [3, 5]. However, with further shift of the phase-transition point down to lower temperatures, a clear first-order transition nature is revealed. Traditional mean-field analysis of the compositional dependence of the thermodynamic potential coefficients, performed for $Sn_2P_2(Se_xS_{1-x})_6$ mixed crystals [11, 12], can be complicated for $(Pb_ySn_{1-y})_2P_2S_6$ solutions. Indeed, in the latter case the compositional dependence of the coefficients is nonlinear.

As has been shown earlier [22, 23] by the analysis of the temperature dependences of the $Sn_2P_2Se_6$ crystals heat capacity, dielectric susceptibility, and wave number of modulation across the incommensurate phase for $Sn_2P_2(Se_xS_{1-x})_6$ crystal, higher-order (eighth and tenth) invariants in the Landau expansion should be taken into consideration. Such nonlinearity is related to the presence of the three-well local potential. Evidently, these higher-order invariants or the linear temperature dependence of the γ coefficient [23] can be taken into account for better fitting of the temperature anomalies of the sound velocity in $(Pb_ySn_{1-y})_2P_2S_6$ crystals and avoiding

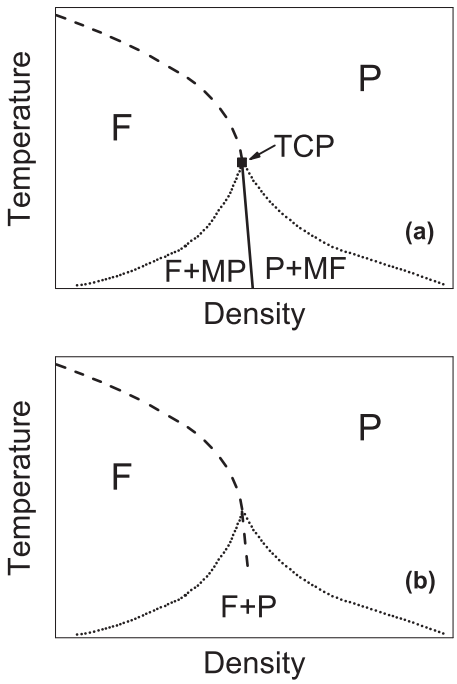

Figure 12 Effect of randomness on the phase diagram with a tricritical point: (a) Phase diagram of a nonrandom system [3] with paraelectric (P), ferroelectric (F), metastable paraelectric (MP), and metastable ferroelectric (MF) phases. Dashed and solid lines indicate the second- and first-order transitions, respectively. Dotted lines show boundaries of the metastable paraelectric and ferroelectric phases. (b) Phase diagram of a random system [5]. Dashed line indicates the second-order transition, dotted lines denote the boundaries of a paraelectric and ferroelectric phase coexistence.

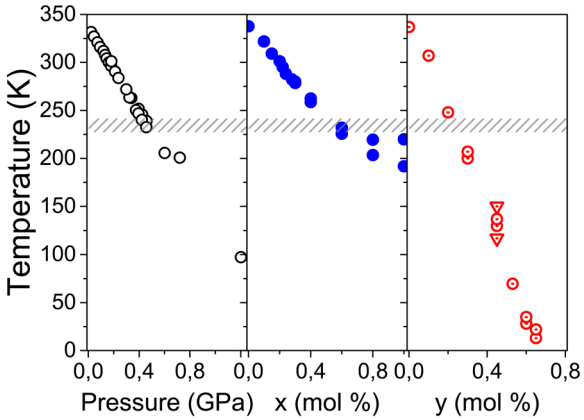

Figure 13 Open symbols (left) show the pressure dependence of the phase-transition temperature in $Sn_2P_2S_6$ crystal based on neutron diffraction [9] and X-ray diffraction [10] data. Solid symbols (center) denote the compositional dependence of the phase-transition temperature in $Sn_2P_2(Se_xS_{1-x})_6$ crystals with an intermediate incommensurate phase at $x > 0.28$ [11, 12]. Compositional dependence of the phase-transition temperature of $(Pb_ySn_{1-y})_2P_2S_6$ crystals is shown by dotted symbols (right; see Fig. 1 for details). The horizontal-shaded bar shows the "waterline temperature" that coincides with the tricritical point positions in the T–P, T–x, and T–y diagrams.

the nonmonotonous dependence of the β and γ coefficients on the lead concentration (Fig. 11).

The observed location of the TCPs at the same temperature level ("the waterline temperature") for different mechanical or chemical impacts (on compression of $Sn_2P_2S_6$ and at S→Se or Sn→Pb substitution) (Fig. 13) can be explained in the following way. On substitution of sulfur by selenium, intercell interaction becomes weaker as a result of the stronger covalence of the chemical bonds [24, 25], but the stereoactivity of the Sn^{2+} cations and the form of the local potential obviously remain almost unchanged. These factors, mostly the intercell interaction weakening, determine the second-order PT temperature decrease until the TCP is reached.

For pure $Sn_2P_2S_6$ crystal under pressure, the Sn^{2+} cations stereoactivity decreases, which reduces the depth of the side wells in the local three-well potential. Due to this factor, at almost unchanged intercell interaction, the second-order PT temperature goes down until the TCP "waterline temperature" and a first-order ferroelectric transition line appears in the T–P diagram.

On the substitution of tin by lead, the sublattice of rather strongly stereoactive Sn^{2+} cations is diluted by weakly stereoactive Pb^{2+} cations, which also have bigger ionic radius. In addition to the dilution effect, the ionicity of the Sn–S chemical bonds increases [24] and the stereoactivity of the remaining Sn^{2+} cations decreases. The combined influence of the intercell interaction strengthening and the decrease of the stereoactivity of the two cation sublattices determines the decrease of the second-order ferroelectric PT temperature down to the above-mentioned "waterline temperature" of the TCPs.

For pure $Sn_2P_2S_6$ lattice compression, the observed T–P phase diagram can be related to the one predicted by the BEG model [2–4]. With substitution of sulfur by selenium, the random field defects can appear but their influence is smoothed: no smearing of very sharp critical anomalies at the phase transitions was observed in the $Sn_2P_2(Se_xS_{1-x})_6$ mixed crystals [26]. This is evidently related to the continuous spatial distribution of the electronic density in the $[P_2S(Se)_6]^{4-}$ anionic groups. Evidently, for these mixed crystals the BEG model can be appropriate in combination with the known ANNNI model [27, 28] that explains the frustration effects and intermediate incommensurate phase appearance at $x > x_{LP} \approx 0.28$ [15].

For the case of substitution of tin by lead, strong random-field defects appear due to hybridization of different electronic orbitals around the Sn^{2+} and Pb^{2+} cations. Such a complicated situation can be described by comparing the experimentally built T–y diagram with the diagram predicted by the diluted BEG model [5].

4 Conclusions For ferroelectric systems, this is the first confirmation of the most important conclusion of the BEG model on the mandatory change of a second-order phase transition into a first-order one (i.e., a TCP should

be achieved) as the transition temperature decreases to a certain value. Such transformation of the phase-transition character is related to the temperature evolution of the free-energy functional in the case of the three-well potential energy profile in the crystals of the $Sn_2P_2S_6$ family, which could be varied by hydrostatic compression or by composition of $Sn_2P_2(Se_xS_{1-x})_6$ or $(Pb_ySn_{1-y})_2P_2S_6$ mixed crystals. Under compression, the temperature of the second-order transition from the paraelectric to the ferroelectric phase decreases: below 250 K and between 0.4 and 0.6 GPa, the tricritical pint was observed experimentally in $Sn_2P_2S_6$ crystals [8, 10]. At a similar temperature level, or near the "waterline temperature" of 250 K, the TCP is revealed for the paraelectric–ferroelectric transition in the $Sn_2P_2(Se_xS_{1-x})_6$ mixed crystal with selenium content $x \approx 0.6$ [11, 12]. From hypersound, ultrasound, and dielectric studies of $(Pb_ySn_{1-y})_2P_2S_6$ mixed crystals, it was found that the TCP can also be achieved as the phase-transition temperature decreases to the "waterline temperature" as the lead concentration increases above $y = 0.2$. At higher lead content, a broad temperature hysteresis of the phase transitions as well as coexistence of phases are observed. $(Pb_ySn_{1-y})_2P_2S_6$ mixed crystals represent a disordered ferroelectric system that can be described by the BEG model with random fields.

Acknowledgements We are grateful to Yuriy Azhniuk for useful discussions and critical reading of the manuscript.

References

[1] K. Z. Rushchanskii, Y. M. Vysochanskii and D. Strauch, Phys. Rev. Lett. **99**, 207601 (2007).
[2] M. Blume, V. J. Emery, and R. B. Griffiths, Phys. Rev. A **4**, 1071 (1971).
[3] C. Ekiz, M. Keskin, and O. Yalçin, Physica A **293**, 215 (2001).
[4] W. Hoston and N. Berker, Phys. Rev. Lett. **67**, 1027 (1991).
[5] A. Falicov and A. N. Berker, Phys. Rev. Lett. **76**, 4380 (1996).
[6] R. S. Solanki, S. K. Mishra, Y. Kuroiwa, C. Moriyoshi, and D. Pandey, Phys. Rev. B **88**, 184109 (2013).
[7] M. D. Glinchuk, E. A. Eliseev, V. A. Stephanovich, and L. Jastrabik, arXiv:cond-mat/0007171v1.
[8] Y. M. Vysochanskii, A. A. Kohutych, A. V. Kityk, A. V. Zadorozhna, M. M. Khoma, and A. A. Grabar, Ferroelectrics **399**, 83 (2010).
[9] P. Ondrejkovic, M. Kempa, Y. Vysochanskii, P. Saint-Gregoire, P. Bourges, K. Z. Rushchanskii, and J. Hlinka, Phys. Rev. B **86**, 224106 (2012).
[10] P. Ondrejkovic, M. Guennou, M. Kempa, Y. Vysochanskii, G. Garbarino, and J. Hlinka, J. Phys.: Condens. Matter **25**, 115901 (2013).
[11] Y. Vysochanskii, M. Maior, V. Rizak, V. Slivka, and M. Khoma, Sov. Phys. JETP **45**, 1355 (1989).
[12] Y. Vysochanskii and V. Slivka, Sov. Phys. Usp **35**, 123 (1992).
[13] C. D. Carpentier and R. Nitsche, Mater. Res. Bull. **9**, 401 (1974).
[14] R. Becker, W. Brockner, and H. Schafer, Z. Naturforsch. **38a**, 874 (1983).
[15] Y. M. Vysochanskii, T. Janssen, R. Currat, R. Folk, J. Banys, J. Grigas, and V. Samulionis, Phase Transitions in Ferroelectric Phosphorous Chalcogenide Crystals (Vilnius University Publishung House, Vilnius, 2006), p. 453.
[16] K. Moriya, K. Iwauchi, M. Ushida, A. Nakagawa, K. Watanabe, S. Yano, S. Motojima, and Y. Akagi, J. Phys. Soc. Jpn. **64**, 1775 (1995).
[17] D. A. Kiselev, K. Z. Rushchanskii, I. K. Bdilin, M. D. Malinkovich, Y. N. Parkhomenko, and Y. M. Vysochanskii, Ferroelectrics **438**, 55 (2012).
[18] R. M. Yevych, Y. M. Vysochanskii, M. M. Khoma, and S. I. Perechinskii, J. Phys.: Condens. Matter **18**, 4047 (2006).
[19] A. A. Kohutych, R. M. Yevych, S. I. Perechinskii, V. Samulionis, J. Banys, and Y. M. Vysochanskii, Phys. Rev. B **82**, 054101 (2010).
[20] L. D. Landau, and I. M. Khalatnikov, Dokl. Akad. Nauk SSSR **96**, 469 (1954).
[21] A. A. Kohutych, R. M. Yevych, S. I. Perechinskii, and Y. M. Vysochanskii, Cent. Eur. J. Phys. **8**, 905 (2010).
[22] V. Y. Korda, S. V. Berezovsky, A. S. Molev, L. P. Korda, and V. F. Klepikov, Physica B **407**, 3388 (2012).
[23] V. Y. Korda, S. V. Berezovsky, A. S. Molev, L. P. Korda, and V. F. Klepikov, Physica B **425**, 31 (2013).
[24] D. Baltrunas, R. Mikaitis, V. Slivka, and Y. Vysochanskii, Phys. Status Solidi A **119**, 71 (1990).
[25] Y. M. Vysochanskii, D. Baltrunas, A. A. Grabar, K. Mazeika, K. Fedyo, and A. Sudavicius, Phys. Status Solidi B **246**, 1110 (2009).
[26] A. Olega, A. Salazar, A. A. Kohutych, and Y. M. Vysochanskii, J. Phys.: Condens. Matter **23**, 025902 (2011).
[27] W. Selke, Phys. Rep. **170**, 213 (1988).
[28] T. Tome and S. R. Salinas, Phys. Rev. A **39**, 2206 (1989).